Supplementary Information

for

TMSI-TOP: A dual-function precursor for anion exchange and surface passivation via phosphonium iodide formation in $CsPb(Br/I)_3$ perovskite nanocrystals

Seungmin Baek,[†a] Hyeon Woo Jeong,[†a] Hyejin Na,[a] Ansoon Kim,[bc] Seungwook Choi,[bc], Jinseok Lee,[ad] Seon Joo Lee,[ad] Sungho Choi,[a] and Jaemin Lee[*ad]

[a]Advanced Materials Division, Korea Research Institute of Chemical Technology, Yuseong-gu, Daejeon, 34114, Korea

[b]Interdisciplinary Materials Measurement Institute, Korea Research Institute of Standards and Science, Yuseong-gu, Daejeon, 34113, Republic of Korea

[c]Applied Measurement Science, University of Science and Technology, Yuseong-gu, Daejeon, 34113, Republic of Korea

[d]KRICT School, University of Science and Technology, Yuseong-gu, Daejeon, 34113, Republic of Korea

[†]These are equally contributed.

*Corresponding Author: Jaemin Lee (jminlee@krict.re.kr)

Table of Contents

1. Photoluminescence characteristics of PeNCs

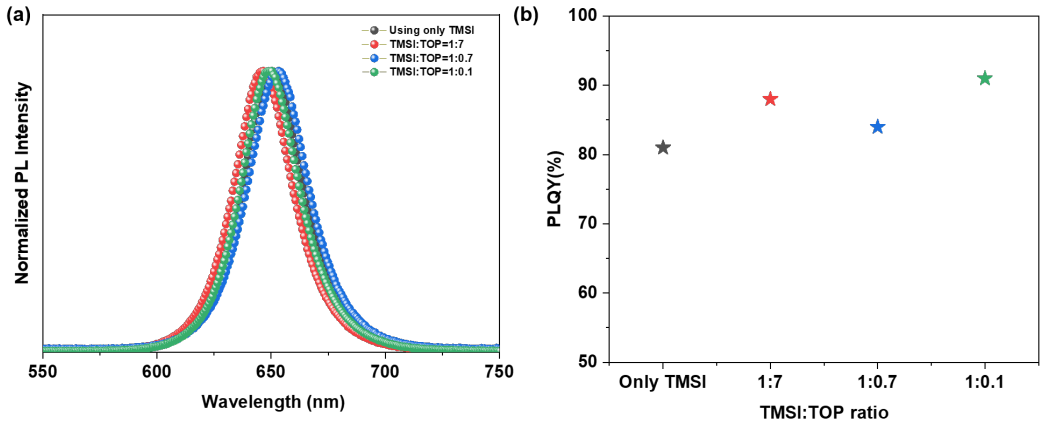

Fig. S1. (a) PL spectra and (b) PLQY as a function of the TMSI:TOP ratio

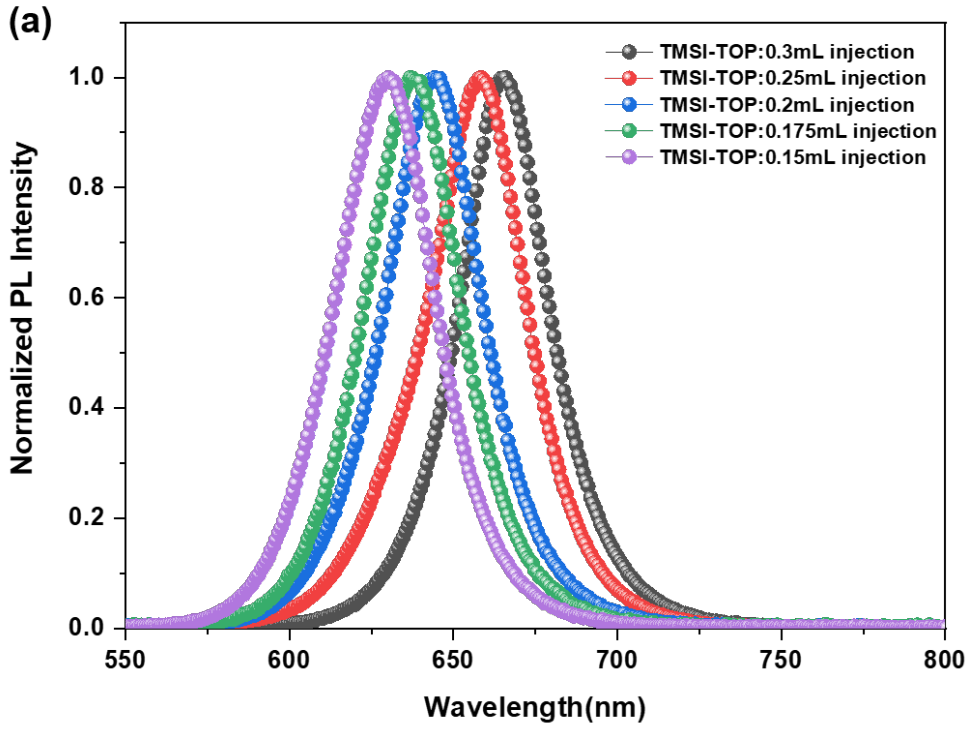

Fig. S2. PL wavelength shift as a function of TMSI–TOP injection amount

2. High-Resolution Transmission Electron Microscopy of PeNCs

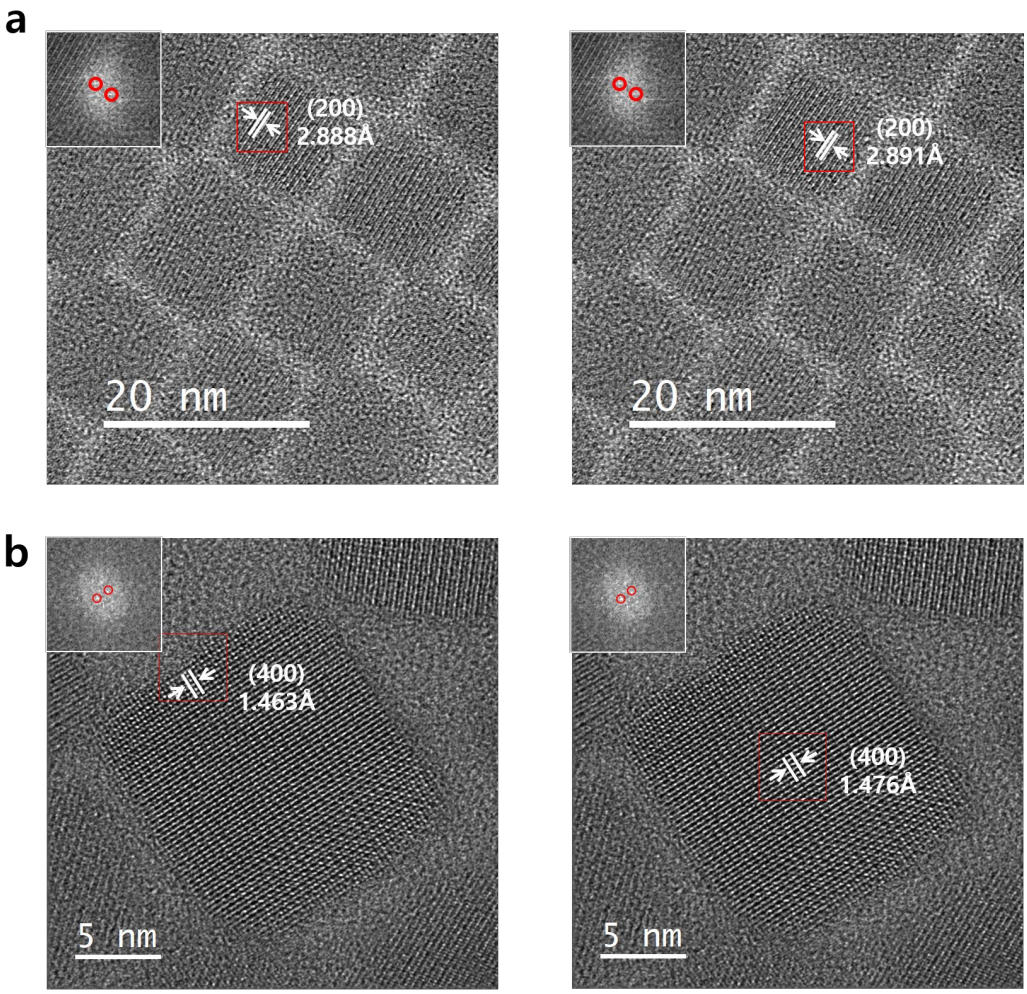

Fig. S3. Comparison of the distance between the center and side planes after anion exchange using HR-TEM. (a) (200) facet. (b) (400) facet.

3. Energy Dispersive X-ray Spectroscopy (EDS) mapping of PeNCs

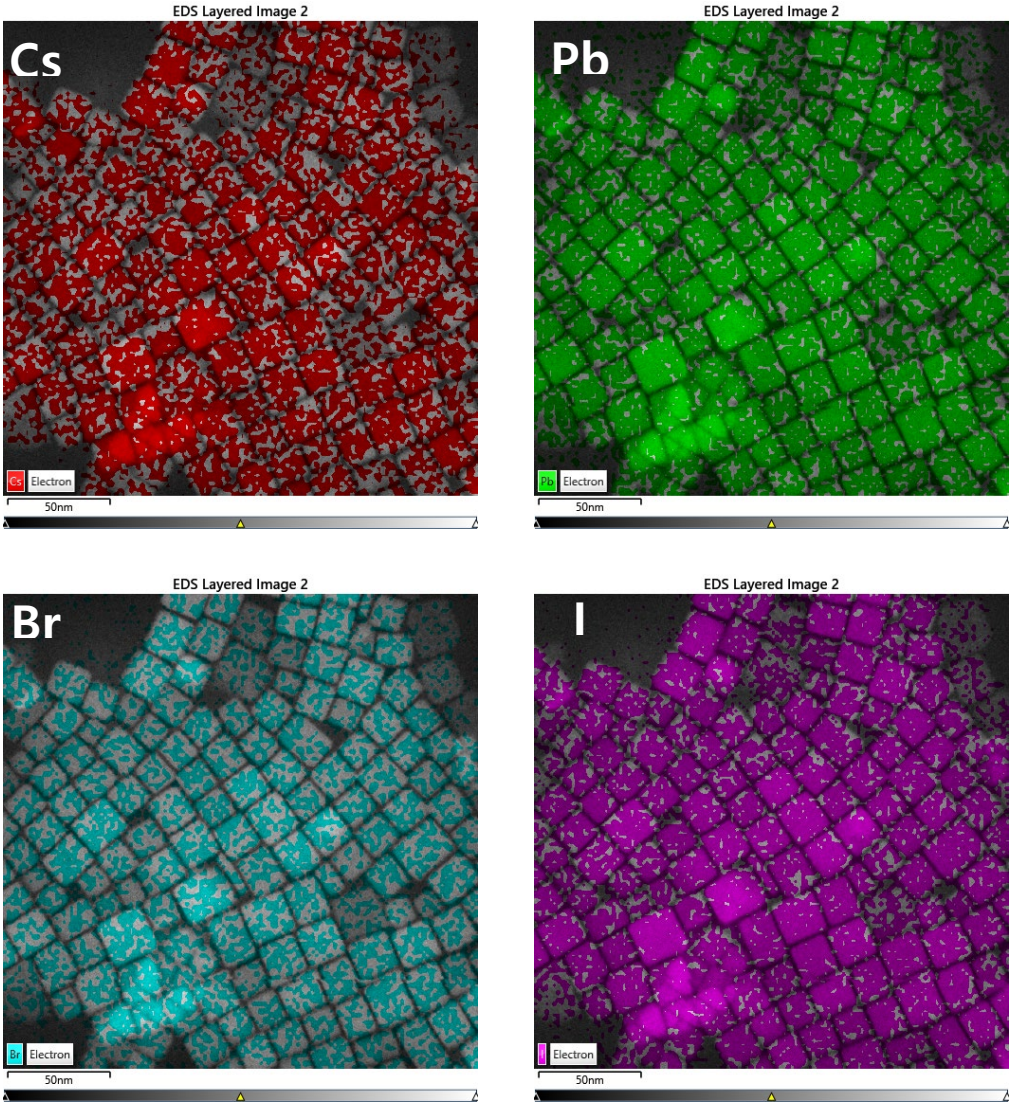

Fig. S4. Energy-dispersive X-ray spectroscopy (EDS) mapping data to investigate the precise halide composition distribution after the anion-exchange reaction.

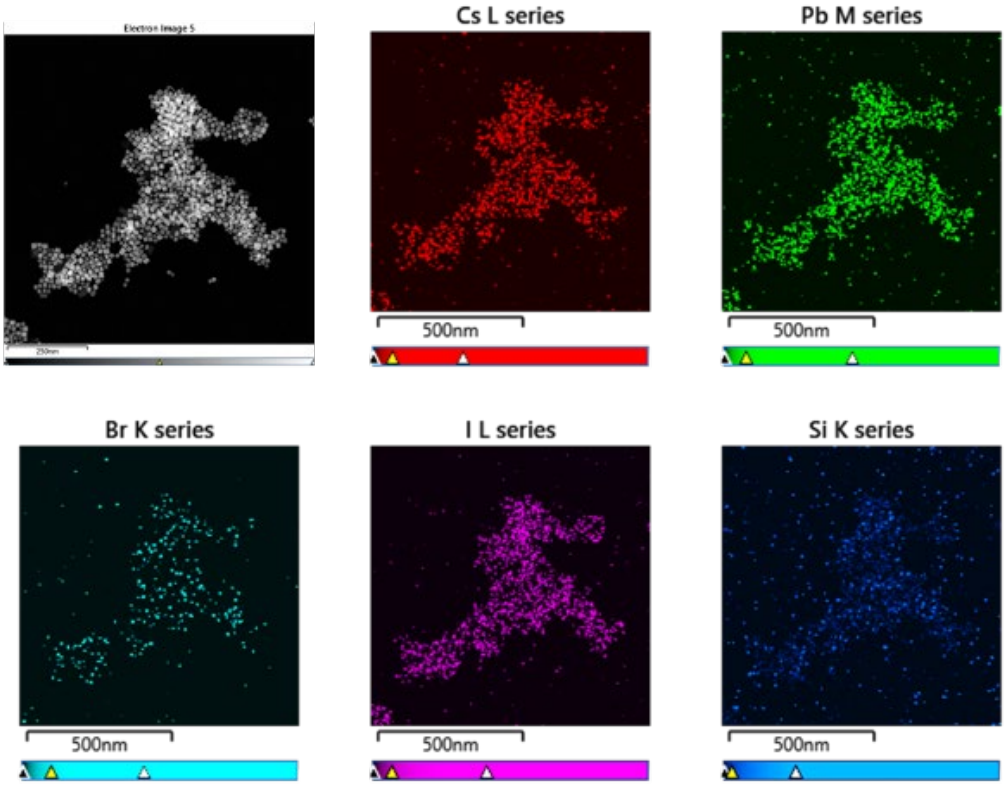

Fig. S5. EDS mapping data showing the surface distribution of Si ions after anion exchange with TMSI-TOP.

4. Photographic images of TMSI-TOP mixtures

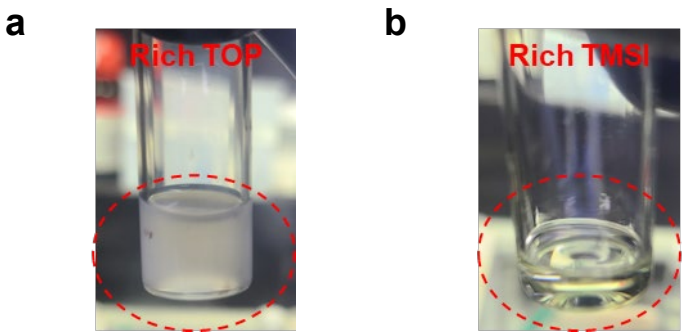

Fig. S6. Photographic images of TMSI-TOP mixtures with (a) a TOP-rich composition and (b) a TMSI-rich composition.

5. PLQY and TCSPC characteristics of PeNCs

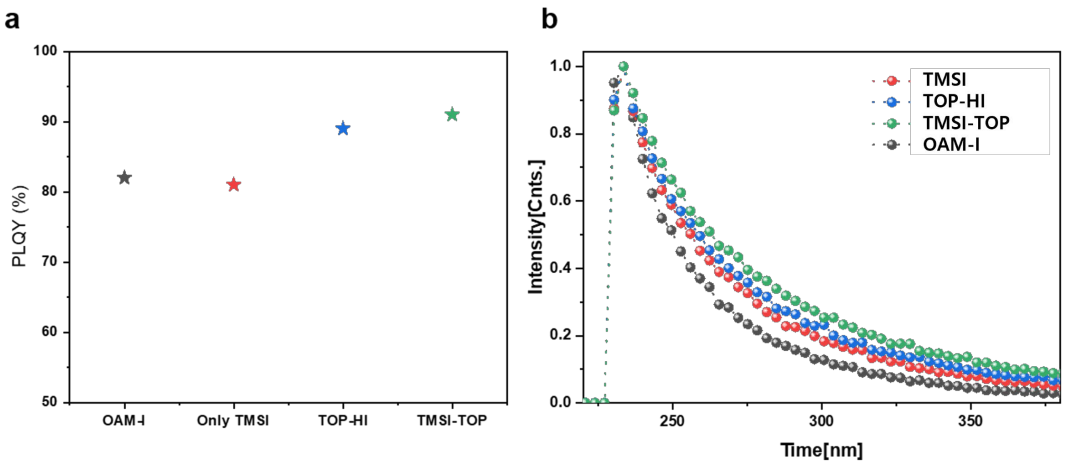

Fig. S7. Comparison of (a) PLQY and (b) TCSPC data of PeNCs synthesized using different anion precursors.

Table S1. Fitting parameters for the decay profiles of the PeNCs samples.

	A_1 [kCnts/Chnl]	T_1 [ns]	A_2 [kCnts/Chnl]	T_2 [ns]	T_{avg} [ns]
OAM-I	1	91.4	5.76	29.3	51.1
TMSI	0.74	137.8	6.47	40.8	67.8
TOP-HI	0.837	152.6	5.957	45.3	79.7
TMSI-TOP	0.99	153.4	6.24	50.6	83.9

6. XPS analysis results of PeNCs

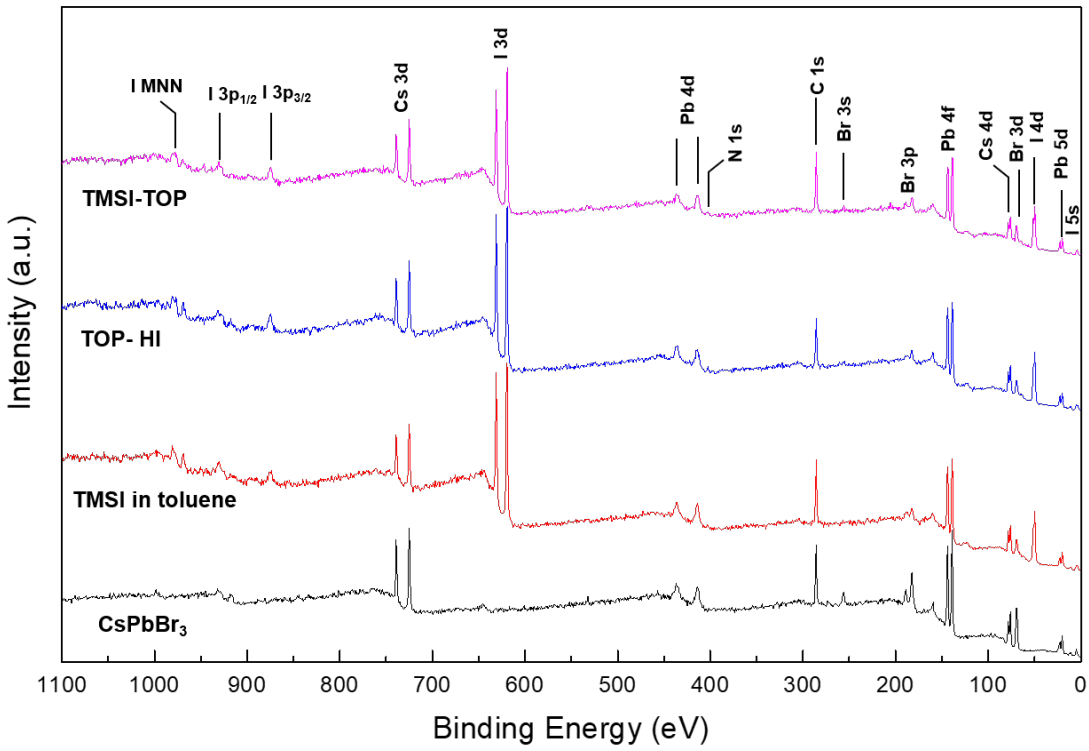

Fig. S8. Comparison of XPS survey scans of PeNC synthesized using each precursor.

Fig. S8 presents the XPS survey spectra of PeNC samples synthesized using different precursors. The survey spectra show the characteristic photoelectron signals corresponding to the primary constituent elements of PeNC, confirming successful anion exchange with iodine. Si and O signals are only detected in the high-resolution core-level spectra (Fig. 3a and Fig. 3b) due to their low surface concentrations and the limited sensitivity of survey spectra.

Table S2 summarizes the elemental compositions obtained from XPS survey spectra (Fig. S8) measured on three different surface areas for each PeNC sample. Quantitative analysis

was performed by calibrating the measured photoelectron intensities using an analyzer transmission function derived following reference procedures.[1, 2] The transmission function was determined using reference foils of Ag, Au and Cu (SCAA90, National Physical Laboratory, UK). Table S3 presents elemental compositions obtained from high-resolution core-level XPS measurements shown in Figs. 3a-c. In contrast to the survey spectra, Si and O core-level signals are clearly resolved in the narrow scan spectra (Fig. 3a and Fig. 3b), enabling their inclusion in the quantitative analysis.

Table S2. Elemental composition derived from XPS survey spectra acquired from three different surface areas using an intensity-scale calibrated transmission function.

Sample	Atomic ratio (%)				(Br+I)/Pb
	Br 3d	I $3d_{5/2}$	Cs $3d_{5/2}$	Pb 4f	
$CsPbBr_3$	61.19	0	16.84	21.97	2.79
	61.85	0	15.9	22.25	2.78
	61.25	0	16.38	22.37	2.74
TMSI with toluene	27.96	38.51	12.13	21.99	3.02
	27.07	37.51	13.46	21.96	2.94
	26.87	36.81	14.75	21.57	2.95
TOP-HI	27.31	36.26	15.13	21.30	2.98
	26.83	36.31	15.18	21.68	2.91
	27.35	35.74	15.15	21.76	2.90
TMSI-TOP	30.3	34.16	14.49	21.05	3.06
	30.44	34.24	14.25	21.07	3.07
	31.26	34.21	14.49	21.2	3.09

Table S3. Elemental composition obtained from narrow scanned XPS results (Fig. 3)

Sample	Atomic ratio (%)					
	Si 2p	Br 3d	I $3d_{5/2}$	Cs $3d_{5/2}$	Pb 4f	O 1s
$CsPbBr_3$	0	61.43	0	16.37	22.20	0
TMSI with toluene	1.76	26.20	36.09	12.90	20.96	2.10
TOP-HI	0	27.95	35.62	14.99	21.45	0
TMSI-TOP	5.43	26.94	30.05	12.66	18.54	6.39

7. Photoluminescence stability test of PeNC films under ambient conditions

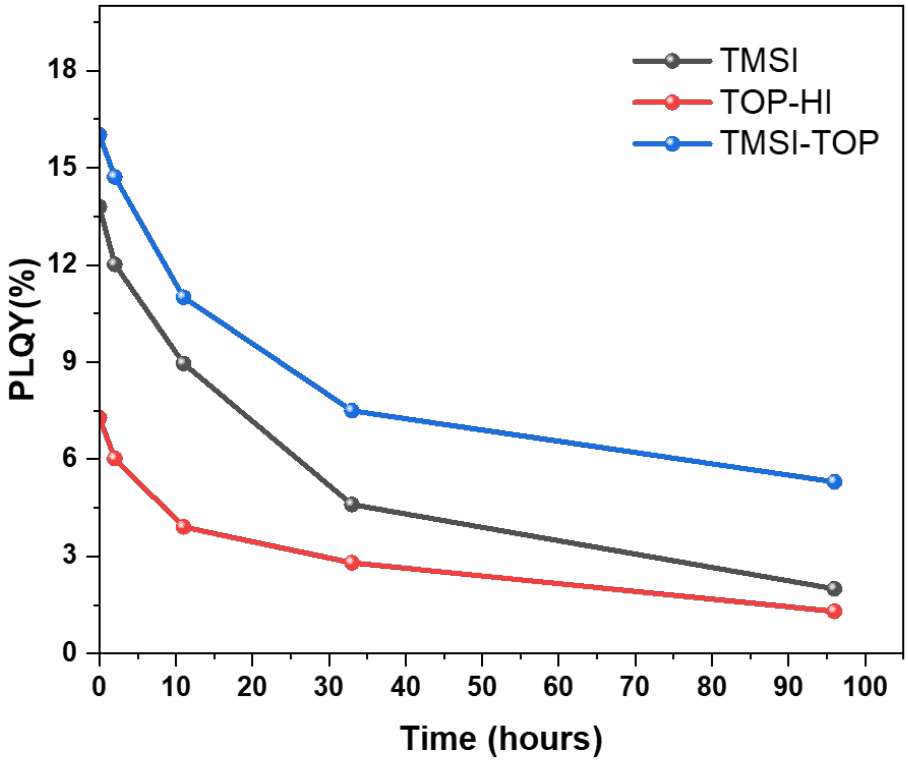

Fig. S9. Stability test of PeNC films synthesized with different anion-exchange precursors in ambient air

8. Perovskite LED characteristics

Table S4. Summary of stability of red-emitting PeNC LED devices at 620-650nm.

Ref	Stability (min)	Stability measurement conditions	Device structure
Our work	**924**	**100 cd/m^2**	**ITO / PEDOT:PSS / PTAA / $CsPb(Br/I)_3$ / TPBi / LIF / Al**
[3]	1200	200 cd/m^2	ITO / PEDOT:PSS / Poly-TPD / $CsPb(Br/I)_3$ / CNT2T / LiF / Al
[4]	786	100 cd/m^2	ITO / PEDOT:PSS / PTAA / DPPA-$CsPb(Br/I)_3$ / TPBi / LIF / Al
[5]	600	200 cd/m^2	ITO / PEDOT:PSS / Poly-TPD / $CsPbI_3$ / TPBi / LiF / Al
[6]	340	0.1 mA/cm^2	ITO / PEDOT:PSS / Poly-TPD / TFB / $MAPb(I/Br)_3$ / TPBi / LiF / Al
[7]	336	245.9 mA/cm^2	ITO / PEDOT:PSS / Poly-TPD / ($CsPbI_3$ SQD-P + T) / TPBi / LiF / Al
[8]	230	100 cd/m^2	ITO / ZnO / PEI / OPA:K-$CsPb(Br/I)_3$ / TCTA / TAPC / MoO_3 / Au
[9]	145	100 cd/m^2	ITO / ZnO / PEI / $GA_{0.28}Cs_{0.72}Pb_{0.40}Ge_{0.55}Cd_{0.05}I_3$ / TCTA / MoO_x / Ag
[10]	97	100 cd/m^2	ITO / PEDOT:PSS / Poly-TPD / BS-NCs / TPBi / LiF / Al
[11]	95	107 cd/m^2	ITO / PEDOT:PSS / Poly-TPD / $CsPbI_3$ / TPBi / LiF / Al
[12]	70	150 cd/m^2	ITO / PEDOT:PSS / Poly-TPD / CPIBr-D+T / TPBi / LiF / Al
[13]	63	100 cd/m^2	ITO / PEDOT:PSS / Poly-TPD / TRP_NCs $CsPb(Br/I)_3$ / TPBi / LiF / Al
[14]	13.3	100 cd/m^2	ITO / PEDOT:PSS / PTAA / KI-$CsPb(Br/I)_3$ / TPBi / LIF / Al
[15]	5	0.7 V	ITO / PEDOT:PSS / Poly-TPD / $CsPb(Br/I)_3$ / TPBi / Liq / Al

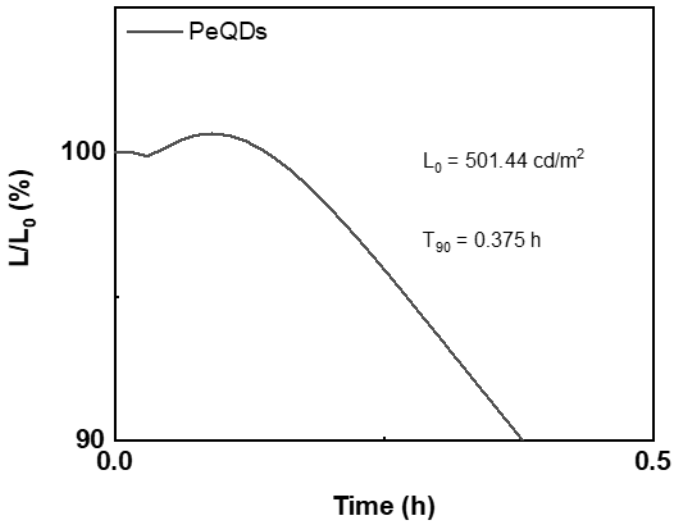

Fig. S10. LT_{90} lifetime at 500 cd/m²

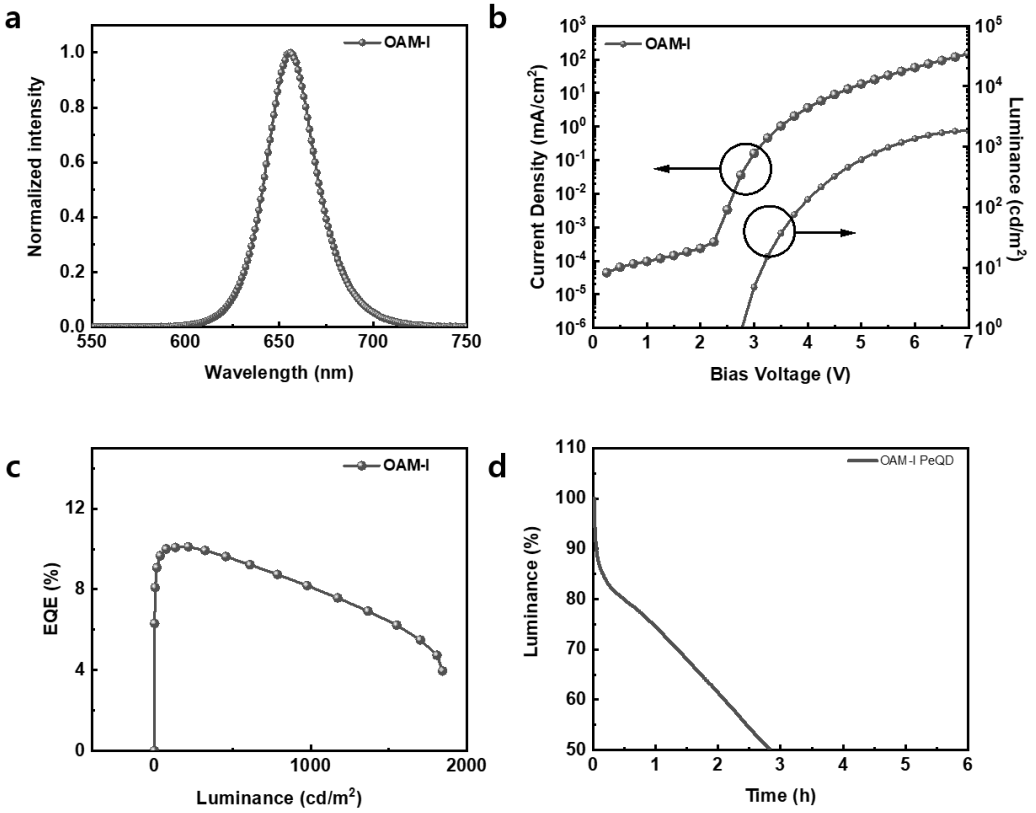

Fig. S11. Device characterization results. a) EL spectra of PeNC using OAM-I. b) J-V-L curve. c) EQE-Luminance curve. d) Operation lifetime curve.

9. Hole-only device (HOD) characteristics

In the single-carrier devices, the trap density (N_{trap}) is calculated from the trap-filled limit voltage (V_{TFL}) by using an equation derived from the current behavior in the trap-filled limit region:

$$N_{trap} = \frac{2\varepsilon\varepsilon_0 V_{TFL}}{eL^2} \qquad (1)$$

where ε is the dielectric constant of $CsPb(Br/I)_3$ (8.6),[16, 17] ε_0 is the vacuum permittivity (8.854 x 10^{-12} C $V^{-1}m^{-1}$), V_{TFL} is the trap-filled limit voltage, L is the thickness of the film and e is the electric charge (1.6 x 10^{-19} C). The sharp increase in current around V_{TFL} is directly related to the number of available traps in the material. By measuring the current and bias at V_{TFL}, the trap density can be determined. This relationship is based on the assumption that the trap density influences the carrier transport and the filling of traps as voltage is applied. The device structure of the hole-only devices were ITO /PEDOT: PSS (30nm) /PeNCs (85 nm) /MoO_3 (7 nm) /Au (100 nm), and the measured electrical characteristics are shown in Fig. S7. Thus, the trap density (N_{trap}) could be obtained by analyzing the current-voltage data, particularly focusing on the transition around the V_{TFL}, where the behavior shifts due to the influence of traps on charge transport. The measured V_{TFL} values for the three hole-only devices were 2.30 V, 1.62 V, and 1.01 V for the TMSI in toluene, TOP-HI, and TMSI-TOP devices, respectively. The calculated hole trap densities (N_h) of the PeNC films, based on the above equation, were 2.61×10^{18}, 1.84×10^{18}, and 1.14×10^{18} cm^{-3}, respectively, for TMSI in toluene, TOP-HI, and TMSI-TOP PeNCs. The trend of decreasing trap density in each PeNC

film, from TMSI in toluene to TMSI-TOP, is ultimately correlated with the lifetime of the Pe-LED devices, as observed earlier. The lower trap density means fewer surface defects of the PeNCs, which can lead to higher radiative recombination. This also corresponds well to the previous TCSPC analyses. As seen in the UPS results, the shift of the Fermi level closer to the valence band for TMSI-TOP PeNCs implies an increased p-type character, which in turn facilitates more efficient hole transport and enhances charge recombination. Additionally, the hole-only device (HOD) measurements indicated a reduction in trap density, which otherwise blocks hole pathways or shortens hole lifetimes, thereby decreasing transport efficiency. This confirms that the mobility of holes increases as trap density decreases, further supporting the enhanced charge transport properties.

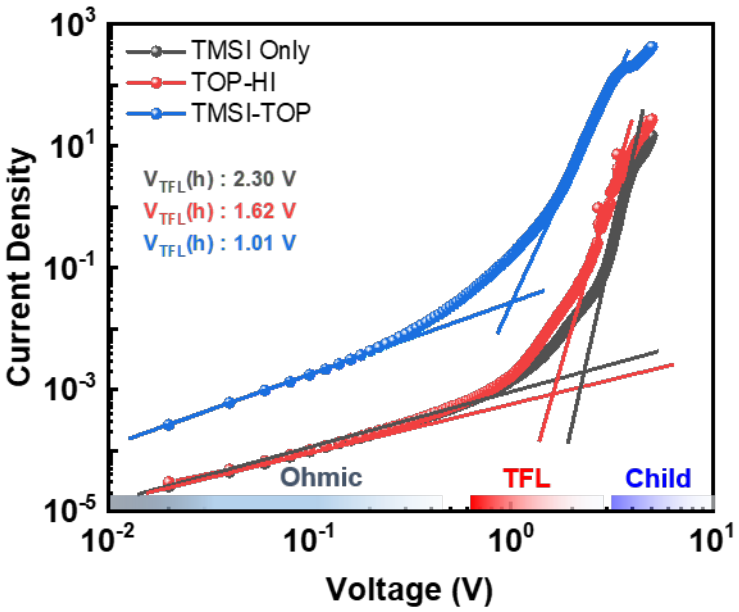

Fig. S12. Space-charge-limited current. J-V characteristics of hole-only devices based on PeNCs synthesized with each anion exchange precursor.

10. External quantum efficiency of Perovskite LEDs

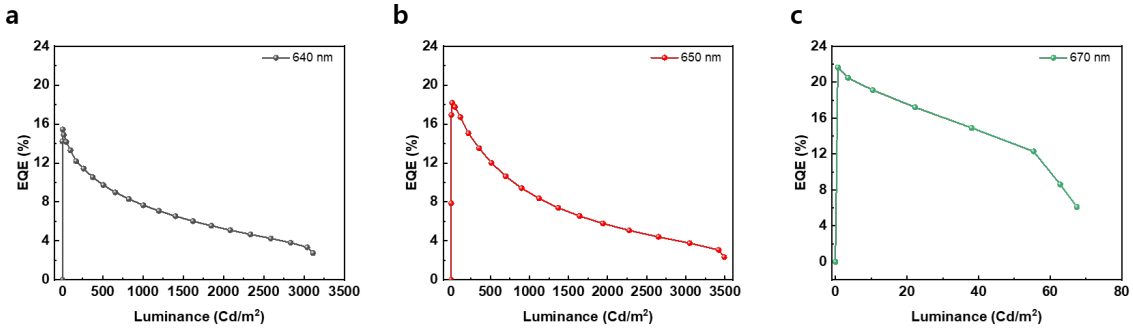

Fig. S13. EQE versus luminance graphs by wavelength. (a) 643nm, (b) 655nm, (c) 669nm.

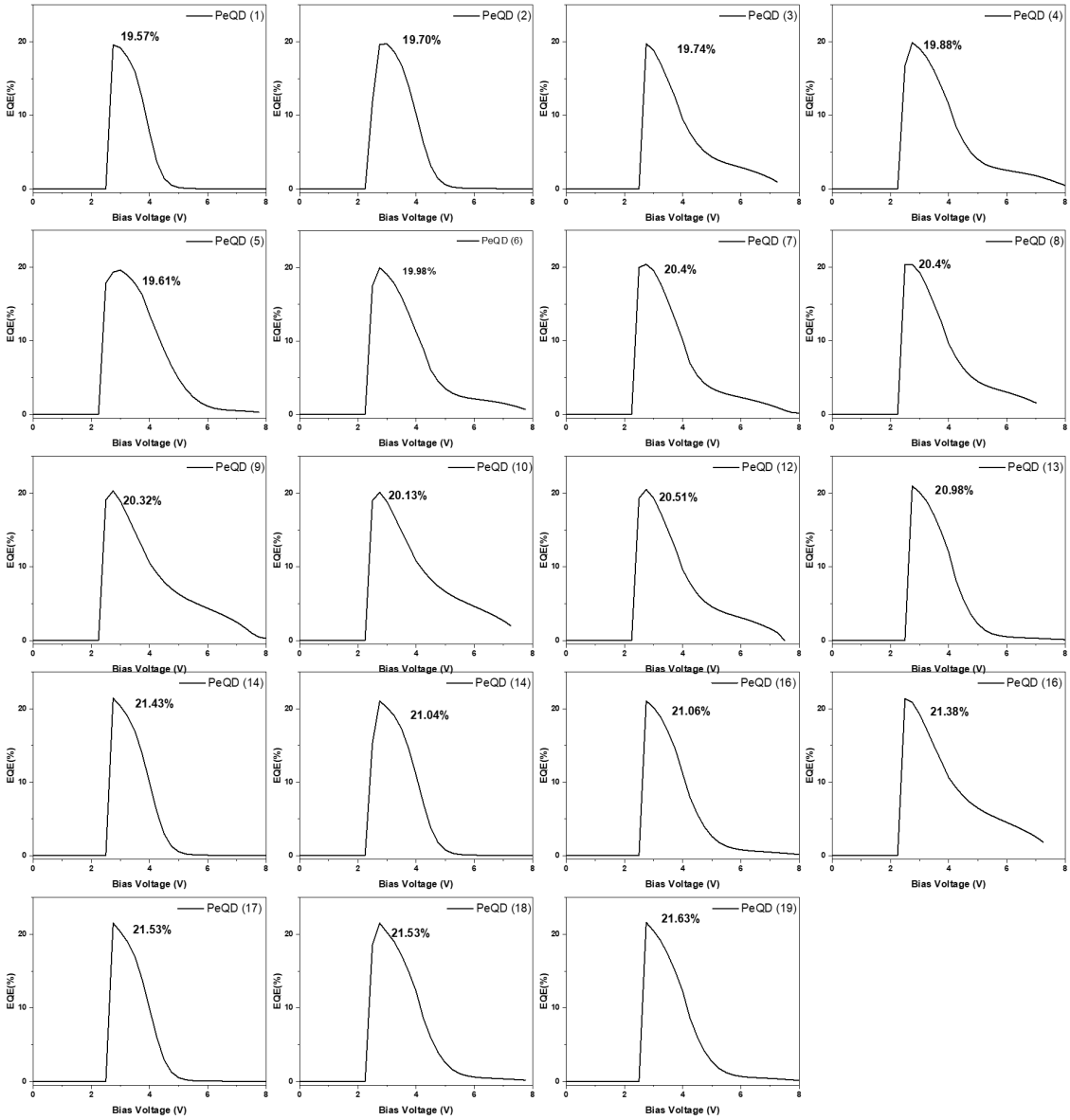

Fig. S14. Raw data: EQE-voltage graphs for each of the 19 devices.

References

[1] M. P. Seah, *Surf. Interface Anal.*, 1993, **20**, 243-266.

[2] M. P. Seah, *J. Electron Spectrosc. Relat. Phenom.*, 1995, **71**, 191-204.

[3] Y.-K. Wang, K. Singh, J.-Y. Li, Y. Dong, X.-Q. Wang, J. M. Pina, Y.-J. Yu, R. Sabatini, Y. Liu, D. Ma, J. Liu, Z. Liu, Y. Gao, O. Voznyy, W. Ma, M.-K. Fung, L.-S. Liao, E. H. Sargent, *Adv. Mater*., 2022, **34,** 21, 2200854.

[4] H. Li, X. Zhu, D. Zhang, Y. Gao, Y. Feng, Z. Ma, J. Huang, H. He, Z. Ye, X. Dai, *Nat. Commun*. 2024, **15**, 6561.

[5] Y.-K. Wang, F. Yuan, Y. Dong, J.-Y. Li, A. Johnston, B. Chen, M. I. Saidaminov, C. Zhou, X. Zheng, Y. Hou, K. Bertens, H. Ebe, D. Ma, Z. Deng, S. Yuan, R. Chen, L. K. Sagar, J. Liu, J. Fan, P. Li, X. Li, Y. Gao, M.-K. Fung, Z.-H. Lu, O. M. Bakr, L.-S. Liao, E. H. Sargent, *Angew. Chem. Int. Ed*. 2021, **60**, 16164–16170.

[6] Y. Hassan, J. H. Park, M. L. Crawford, A. Sadhanala, J. Lee, J. C. Sadighian, E. Mosconi, R. Shivanna, E. Radicchi, M. Jeong, C. Yang, H. Choi, S. H. Park, M. H. Song, F. De Angelis, C. Y. Wong, R. H. Friend, B. R. Lee, H. J. Snaith, *Nature* 2021, **591**, 72–77.

[7] M. Xie, J. Guo, X. Zhang, C. Bi, L. Zhang, Z. Chu, W. Zheng, J. You, J. Tian, High-efficiency pure-red perovskite quantum-dot light-emitting diodes, *Nano Lett.* 2022, **22**, 8266–8273.

[8] P. Lu, M. Lu, F. Zhang, F. Qin, S. Sun, Y. Zhang, W. W. Yu, X. Bai, *Nano Energy* 2023, **108**, 108208.

[9] J. Guo, Y. Fu, W. Zheng, M. Xie, Y. Huang, Z. Miao, C. Han, W. Yin, J. Zhang, X. Yang, J.

Tian, X. Zhang, *Nano Lett*. 2024, **24**, 417–423.

[10] J. Zhang, T. Zhang, Z. Ma, F. Yuan, X. Zhou, H. Wang, Z. Liu, J. Qing, H. Chen, X. Li, S. Su, J. Xie, Z. Shi, L. Hou, C. Shan, *Adv. Mater*. 2023, **35**, 2209002.

[11] J. Guo, M. Xie, H. Li, L. Zhang, L. Zhang, X. Zhang, W. Zheng, J. Tian, *Nano Lett*. 2024, **24**, 6410–6416.

[12] C. Chen, T. Xuan, Y. Yang, F. Huang, T. Zhou, L. Wang, R.-J. Xie, *ACS Appl. Mater. Interfaces* 2022, **14**, 16404–16412.

[13] J. Zhang, B. Cai, X. Zhou, F. Yuan, C. Yin, H. Wang, H. Chen, X. Ji, X. Liang, C. Shen, Y. Wang, Z. Ma, J. Qing, Z. Shi, Z. Hu, L. Hou, H. Zeng, S. Bai, F. Gao, *Adv. Mater*. 2023, **35,** 2303938.

[14] Y. Zhou, T. Fang, G. Liu, H. Xiang, L. Yang, Y. Li, R. Wang, D. Yan, Y. Dong, B. Cai, H. Zeng, Adv. *Funct. Mater*. 2021, **31**, 2106871.

[15] T. Chiba, Y. Hayashi, H. Ebe, K. Hoshi, J. Sato, S. Sato, Y.-J. Pu, S. Ohisa, J. Kido, *Nat. Photonics* 2018, **12**, 11, 681–687.

[16] X. Shen, X. Zhang, Z. Wang, X. Gao, Y. Wang, P. Lu, X. Bai, J. Hu, Z. Shi, W. W. Yu, Y. Zhang, *Adv. Funct. Mater.* 2022, **32**, 2110048.

[17] Z. Yang, A. Surrente, K. Galkowski, A. Miyata, O. Portugall, R. J. Sutton, A. A. Haghighirad, H. J. Snaith, D. K. Maude, P. Plochocka, R. J. Nicholas, *ACS Energy Lett*. 2017, **2**, 1621–1627.